Highest spin discrete levels in ^{131,132}Ce: Spin generation near the mesoscopic limit

E. S. Paul,[1] P. T. W. Choy,[1] C. Andreoiu,[1,*] A. J. Boston,[1] A. O. Evans,[1] C. Fox,[1,†] S. Gros,[1] P. J. Nolan,[1] G. Rainovski,[1,‡] J. A. Sampson,[1] H. C. Scraggs,[1] A. Walker,[1] D. E. Appelbe,[2] D. T. Joss,[2] J. Simpson,[2] J. Gizon,[3] A. Astier,[4,§] N. Buforn,[4] A. Prévost,[4,§] N. Redon,[4] O. Stézowski,[4] B. M. Nyakó,[5] D. Sohler,[5] J. Timár,[5] L. Zolnai,[5] D. Bazzacco,[6] S. Lunardi,[6] C. M. Petrache,[7] P. Bednarczyk,[8] D. Curien,[8] N. Kintz,[8] and I. Ragnarsson[9]

[1]*Oliver Lodge Laboratory, University of Liverpool, Liverpool L69 7ZE, United Kingdom*

[2]*CCLRC Daresbury Laboratory, Daresbury, Warrington WA4 4AD, United Kingdom*

[3]*Institut des Sciences Nucléaires, F-38026 Grenoble, France*

[4]*IPN Lyon, IN2P3-CNRS, Université C. Bernard Lyon-1, F-69622 Villeurbanne, France*

[5]*Institute of Nuclear Research, H-4001 Debrecen, Hungary*

[6]*Dipartimento di Fisica and INFN, Sezione di Padova, I-35131 Padova, Italy*

[7]*Dipartimento di Matematica e Fisica, University of Camerino, via Madonna delle Carceri, I-62032 Camerino, Italy*

[8]*Institut de Recherches Subatomiques, F-67037 Strasbourg, France*

[9]*Department of Mathematical Physics, Lund Institute of Technology, P.O. Box 118, S-22100 Lund, Sweden*

(Received 9 February 2005; published 19 May 2005)

The three superdeformed (SD) bands in ^{132}Ce and the two SD bands in ^{131}Ce have been extended to higher spin, following experiments with the EUROBALL IV spectrometer. The two SD bands in ^{131}Ce have been linked together. However, despite the relatively high population intensity of the bands (up to 5% of the respective channel), it has not been possible to unambiguously link any of the five SD bands into the low-spin, normally deformed structures of ^{131,132}Ce. At the highest spins ($>60\hbar$), some of the bands exhibit the characteristic behavior of smooth band termination, i.e., energetically costly angular-momentum generation near the finite mesoscopic limit. Configuration-dependent cranked Nilsson-Strutinsky calculations have been performed to suggest single-particle configurations for the SD bands and to investigate the possibility of termination in these bands.

DOI: 10.1103/PhysRevC.71.054309 PACS number(s): 27.60.+j, 23.20.Lv, 21.10.Re

I. INTRODUCTION

The generation of angular momentum in atomic nuclei has long been a topical question in nuclear-structure physics. Macroscopically, or classically, deformed nuclei can rotate ever faster to produce a *collective* spin. Microscopically, however, quantal effects of the large, yet finite, ensemble of strongly interacting fermions need to be considered. In the mean-field approximation, each nucleon occupies a quantum state, or *orbital*, with a well defined wave function. Starting with a fully paired (spin 0) doubly magic core, e.g., $^{100}_{50}\mathrm{Sn}_{50}$ or $^{132}_{50}\mathrm{Sn}_{82}$, the addition of valence nucleons can potentially add only a finite amount of angular momentum. The lowest-energy (low-spin) state involves pairwise, time-reversed ($I = 0$) occupation of specific orbitals. A combination of Coriolis and centrifugal forces, induced by rapid rotation, can however break the valence pairs and align the individual nucleonic angular momentum along the "rotation" axis, in accordance with the Pauli exclusion principle. As more pairs are broken, the nucleons contribute more *single-particle* spin to the total angular momentum. With their spin vectors more or less fully aligned along the rotation axis, they tend to polarize the nucleus towards an oblate shape. Eventually, the available spin is exhausted, in which case the total angular momentum is built entirely from particles with their spin vectors quantized along an oblate "rotation axis." Hence, a given nucleus, or rather a specific nucleonic configuration, can only accommodate a limiting value of angular momentum. Experimentally, this effect is seen in γ-ray spectra as *band termination*. The tendencies for different configurations to terminate will, however, be counteracted by mixing between the j shells or the N_{osc} shells, which becomes more important at large deformation. Thus, some configurations might terminate at angular momenta that are larger than expected from their j-shell configurations, while those at even larger deformation will never terminate, see, e.g., Refs. [1,2].

Band termination occurs in many regions of the Segre chart [3,4]. In recent years, a type of *smooth* termination has been observed in the $A \sim 110$ region, which involves a gradual shape change from prolate to oblate over many units of spin [5,6]. In addition to the valence particles outside the $^{100}_{50}\mathrm{Sn}_{50}$ core, an important ingredient of these terminating bands is a two-particle–two-hole (2p–2h) excitation across the spherical $Z = 50$ shell gap, involving $\pi g_{9/2}$ holes. Such excitations induce fairly sizeable prolate quadrupole deformation ($\beta_2 \sim 0.3$) at moderately low spin, and they terminate at $I \sim 50\hbar$ into less deformed, noncollective oblate shapes.

*Present address: Department of Physics, University of Guelph, Guelph, Ontario N1G 2W1, Canada.

†Present address: Triangle Universities Nuclear Laboratory, PO Box 90308, Duke University, Durham, North Carolina 27708-0308.

‡Present address: Department of Physics and Astronomy, SUNY, Stony Brook, New York 11794-3800; on leave from St. Kliment Ohridski University of Sofia, Bulgaria, Sofia 1164, Bulgaria.

§Present address: Centre de Spectrométrie Nucléaire et de Spectrométrie de Masse, Orsay, IN2P3-CNRS, F-91405 Orsay Campus, France.

In the $A \sim 130$ region, superdeformed (SD) bands ($\beta_2 \sim 0.4$) in cerium isotopes are believed to possess similar microscopic proton configurations as the $A \sim 110$ terminating bands [7]. The same proton particle-hole excitations across the $Z = 50$ spherical shell gap, coupled with similar neutron particle-hole excitations across the $N = 82$ shell gap, maintain the superdeformed shape. The holes reside in strongly upsloping (with respect to quadrupole deformation) *extruder* orbitals (e.g., $\pi g_{9/2}$), while the particles occupy strongly downsloping *intruder* orbitals (e.g., $\nu i_{13/2}$ and $\nu h_{9/2}/f_{7/2}$). Thus, smooth band termination might again be expected for these SD bands, although at much higher spin ($\gtrsim 70\hbar$) than in the $A \sim 110$ region, due to the larger valence space. As discussed above, another possibility is that these bands do not terminate, due to the mixing between the *j* shells. In order to test these different scenarios, it is vital to experimentally probe the highest spin states of SD bands in this mass region. The strongly populated (yrast) SD band in ^{132}Ce [8,9] is an ideal candidate for such a study. The present paper also discusses the two excited SD bands in ^{132}Ce [10] and the two SD bands in neighboring ^{131}Ce [11–13], all of which have been extended to higher spin.

II. EXPERIMENTAL METHODS AND RESULTS

The experimental elucidation of the highest spin states in nuclei has greatly advanced in recent years with the advent of large, highly efficient multidetector γ-ray spectrometers such as EUROBALL [14,15] and GAMMASPHERE [16]. The addition of a total-energy/fold calorimeter to EUROBALL has further increased its sensitivity to the highest spin states. In this regard, the high-spin structure of ^{131,132}Ce has been studied at the Institut de Recherches Subatomique (IReS), Strasbourg, using the EUROBALL IV γ-ray spectrometer with a bismuth germanate (BGO) inner-ball calorimeter.

The EUROBALL IV spectrometer consists of three types of Ge detector: 15 seven-crystal, hexagonal "cluster" detectors are placed upstream of the target; 30 single-crystal "tapered" detectors are placed downstream; and 26 four-crystal "clover" detectors are placed in two rings around the target position, at angles near 90° to the beam axis. Each of the three sections of Ge detectors has its own inner-ball section: The cluster end consists of 80 hexagonal BGO elements; the tapered end consists of 75 trapezoidal BGO elements; and the clover section contains 26 BGO elements including active collimators. Since the inner-ball coverage is only ~60% of 4π, the Ge detectors, and their BGO anticompton shields, must also be used to construct, event by event, the measured fold k and sum-energy H of the whole EUROBALL IV system. The individual Ge crystals and the BGO elements were grouped together to operate as a 164-element inner ball, (59 from the Ge's and 105 from the BGO's). The grouping was arranged such that each element covered approximately the same solid angle. The experimental fold k is defined as the measured number of γ rays from an event. Similarly, the sum-energy H is defined as the total measured energy of an event deposited in the spectrometer.

Two separate experiments were performed at beam energies of 160 and 165 MeV, respectively, with the Vivitron electrostatic accelerator providing ^{36}S beams to bombard a thin self-supporting foil of ^{100}Mo, of thickness 600 μg/cm^2. A total of 1.5×10^9 events, at the lower beam energy, and 3.6×10^9 events, at the higher beam energy, were recorded. The trigger condition demanded that 8 or more unsuppressed Ge and 10 or more elements of the BGO inner ball fired. After unfolding the data, the average Compton-suppressed γ-ray multiplicity was 4.5.

In the offline analysis, the fold k and sum-energy H were constructed event by event from both the inner ball and the germanium detectors. Examples of triple Ge γ-ray gated fold and sum-energy distributions, obtained from the 160-MeV data, are shown in Fig. 1 compared to the ungated distributions.

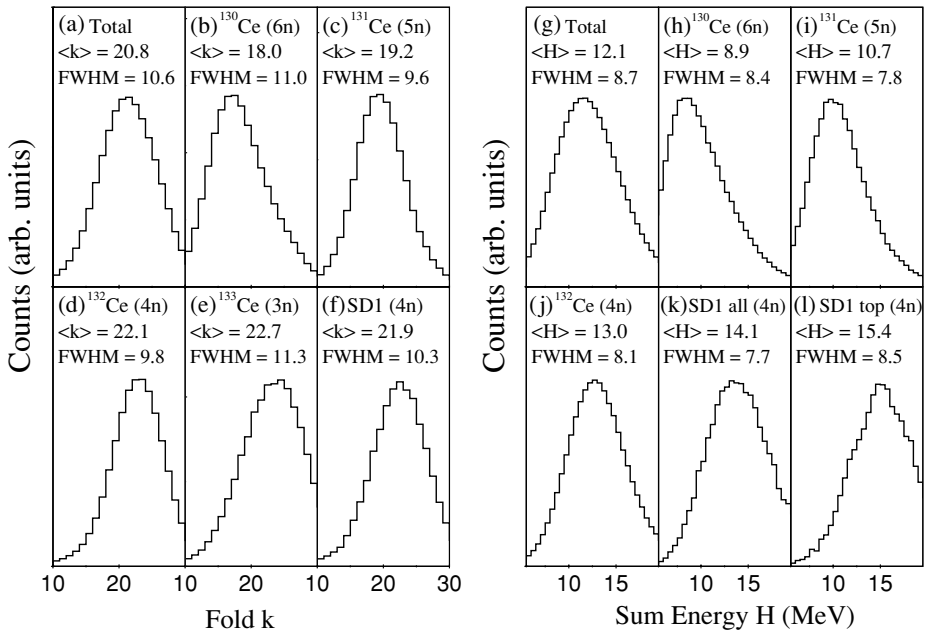

FIG. 1. Fold distributions obtained from the experiment at $E_{\text{beam}} =$ 160 MeV are shown to the left. The total projection of the distribution is shown in (a), while triple-γ-ray gated distributions are shown for low-spin structures in $^{130-133}$Ce (b–e) and for the SD1 band in ^{132}Ce in (f). The measured centroid and width of each distribution is shown. Sum-energy distributions obtained from the experiment at $E_{\text{beam}} =$ 160 MeV are shown to the right. The total projection of the distribution is shown in (g), while triple-γ-ray gated distributions are shown for low-spin structures in $^{130-132}$Ce (h–j) and for the SD1 band in ^{132}Ce in (k, l). The measured centroid and width of each distribution is shown in MeV.

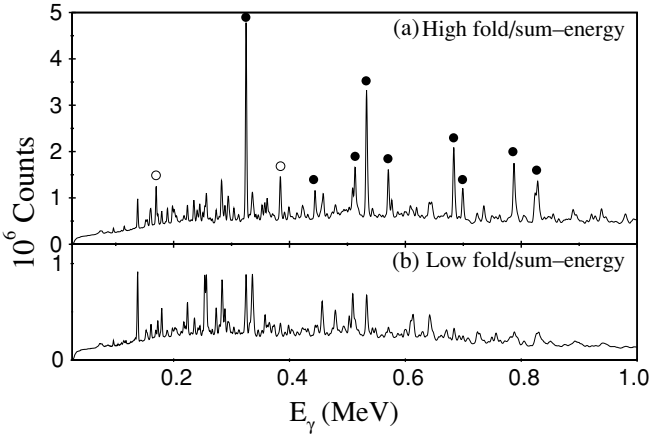

FIG. 2. γ-ray spectra gated by a high $k - H$ condition (a) and a low $k - H$ condition (b). γ rays from ^{132}Ce ($4n$: solid circles) and ^{133}Ce ($3n$: open circles) are clearly enhanced in the high $k - H$ selection relative to the other exit channels, which include ^{131}Ce ($5n$), ^{130}Ce ($6n$), ^{131}La ($p4n$), and ^{128}Ba ($\alpha 4n$).

While the overall, ungated, fold centroid occurs at $\langle k \rangle = 20.8$ [Fig. 1(a)], the centroid changes from 18.0 for ^{130}Ce [$6n$ channel, Fig. 1(b)], through 19.2 for ^{131}Ce [$5n$, Fig. 1(c)], 22.1 for ^{132}Ce [$4n$, Fig. 1(d)], to 22.7 for ^{133}Ce [$3n$, Fig. 1(e)]. For comparison, the fold distribution obtained for the yrast superdeformed band in ^{132}Ce (SD1) is shown in Fig. 1(f). In the case of the sum-energy distributions, the overall (ungated) centroid occurs at $\langle H \rangle = 12.1$ MeV [Fig. 1(g)], while the centroid changes from 8.9 MeV for ^{130}Ce [$6n$ channel, Fig. 1(h)], through 10.7 MeV for ^{131}Ce [$5n$, Fig. 1(i)], and to 13.0 MeV for ^{132}Ce [$4n$, Fig. 1(j)]. Sum-energy distributions corresponding to the yrast SD band in ^{132}Ce are also included in Fig. 1(k, l). The former, with a centroid of 14.1 MeV, used the first 22 (lowest-spin) transitions of the band as gates, while the latter, with a centroid of 15.4 MeV, used only the topmost 8 of these 22 transitions.

The effect of low and high $k - H$ gating is evident in the γ-ray spectra shown in Fig. 2; there is a very clear difference in these spectra with transitions in ^{132}Ce (the $4n$ exit channel) dominating for the high $k - H$ selection, as shown in Fig. 2(a), while the ^{131}Ce ($5n$) and ^{132}Ce ($4n$) transitions have similar strength in the low $k - H$ selection of Fig. 2(b).

For the study of ^{132}Ce, only those events of high fold ($k > 22$) and high sum-energy ($H > 13$ MeV) were considered. In this selection, two-dimensional gates were set in the $k - H$ plane, and approximately 50% of the original data were retained. However, for the study of ^{131}Ce, all events were considered. While a low $k - H$ selection might enhance the population of the low-spin level scheme of ^{131}Ce, the high-spin SD bands should still provide events with high $k - H$ values.

In order to determine transition multipolarities, angular-correlation matrices were constructed by sorting the backward elements of the cluster detectors ($\theta \approx 158^\circ$) against the clover detectors, which are near 90°. An angular intensity ratio

$$R = \frac{I_{\gamma\gamma}(\text{measured } 158^\circ, \text{ gated } 90^\circ)}{I_{\gamma\gamma}(\text{measured } 90^\circ, \text{ gated } 158^\circ)} \qquad (1)$$

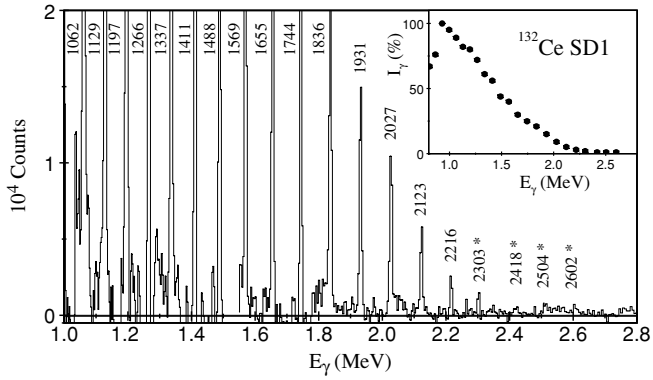

FIG. 3. Double-gated triple-coincidence spectrum generated for SD1 in ^{132}Ce showing the topmost transitions. Transition energies are labeled in keV, and the new transitions are marked with an asterisk. The inset shows the intensity profile of the band.

was then evaluated. Values of $R \approx 1.0$ are expected for a stretched $E2$ quadrupole transition (or a nonstretched dipole transition), and values of $R \approx 0.65$ for pure stretched $M1$ or $E1$ dipole transitions.

A. Results for ^{132}Ce

Approximately 2.8×10^{10} Compton-suppressed quadruple coincident events (γ^4), comprising 7×10^9 events at $E_{\text{beam}} = 160$ MeV and 2.1×10^{10} events at 165 MeV, were unfolded from the high $k - H$ data sets and replayed into a RADWARE-format four-dimensional hypercube [17,18], requiring 20 Gb of disc space, for subsequent analysis. The data were binned corresponding to a constant number of channels (2.5) per γ-ray peak full-width-half-maximum (FWHM), where the FWHM was parametrized as a quadratic function of γ-ray energy [17]. A modified version of the RADWARE graphical-analysis program 4DG8R [19], incorporating the background-subtraction technique of Ref. [20], was used to examine the hypercube. In addition, both one- and two-dimensional spectra, multiply gated by transitions in the known SD bands [8–10], were unfolded directly from the data.

Examples of gated coincidence spectra for the three SD bands in ^{132}Ce are shown in Figs. 3 and 4, while γ-ray energies, intensities, and angular-correlation ratios are listed in Table I, and the bands are drawn in Fig. 5. SD1 has been extended to higher spin by four transitions of energies 2303, 2418, 2504, and 2602 keV; SD2 by six transitions (1621, 1730, 1816, 1907, 1999, and 2086 keV); and SD3 by five transitions (1815, 1885, 1954, 2001, and 2054 keV).

Despite extensive searches, it has not been possible to link unambiguously any of the SD bands into the known low-spin, normally deformed level scheme of ^{132}Ce [21]. SD1 starts to decay from the level fed by the 809-keV transition (Fig. 5) and predominantly feeds the yrast 18^+ normally deformed state of ^{132}Ce, while SD2 and SD3 only feed yrast negative-parity states [22]. We have tentatively chosen $I^\pi = 20^+$ as the most likely bandhead spin of SD1, as shown in Fig. 5; the spins of the other four SD bands in ^{131,132}Ce are then assigned as suggested from "identical" band relationships [13,23].

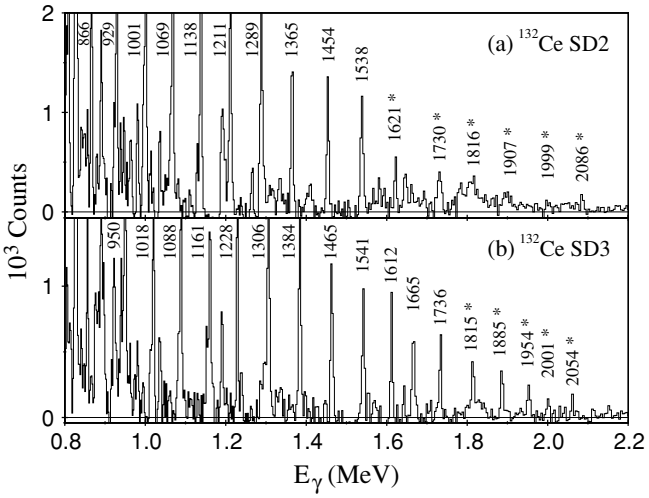

FIG. 4. Double-gated triple-coincidence spectra generated for SD2 (a) and SD3 (b) in ^{132}Ce. Transition energies are labeled in keV, and the new transitions are marked with an asterisk.

B. Results for ^{131}Ce

For the analysis of ^{131}Ce, there were no $k - H$ conditions on the inner ball. Approximately 3.8×10^{10} Compton-suppressed quadruple coincident events were unfolded and replayed into a second hypercube. Examples of gated coincidence spectra for the two SD bands in ^{131}Ce are shown in Fig. 6, while γ-ray energies, intensities, and angular-intensity ratios are listed in Table II, and the bands are included in Fig. 5.

Four new transitions with energies 1831, 1925, 2011, and 2108 keV have been added to the top of ^{131}Ce SD1. Similarly, four new transitions of energies 1813, 1905, 2000, and 2095 keV have been added to the top of ^{131}Ce SD2. In addition, two linking transitions of energies 1514 and 1523 keV have been unambiguously established between these bands. A γ^3 spectrum, gated by the lowest transitions of SD1 (591, 662, and 733 keV) simultaneously with all the transitions of SD2, is shown in Fig. 7 and clearly shows the two linking transitions. The angular intensity ratios extracted for the linking transitions ($\sim$1.9) are too large for them to be stretched $E2$ quadrupole transitions, or indeed stretched ($\Delta I = 1$) or nonstretched ($\Delta I = 0$) $E1$ dipole transitions. The values rather imply mixed $M1/E2$ $\Delta I = 1$ character with large positive multipole mixing ratios $\delta > 0$. The two SD bands in ^{131}Ce are thus determined to have the same parity but opposite signature, $\alpha = I$ mod 2. The two linking transitions do not carry the full intensity of SD2; they each carry only $\sim$10% of the intensity of the 796-keV transition of SD2. A 788-keV transition of similar intensity also depopulates the level fed by the 796-keV transition of SD2, as shown in Fig. 7. It has not been possible, however, to unambiguously link SD2, or indeed SD1, directly into the known low-spin, normally deformed level scheme of ^{131}Ce [21].

TABLE I. Measured γ-ray energies, relative intensities, and angular intensity ratios for the SD bands in ^{132}Ce. The absolute intensity of SD1 is $\approx$6% of the $2^+ \rightarrow 0^+$ transition of ^{132}Ce, while SD2 and SD3 are both $\approx$1%.

^{132}Ce SD1			^{132}Ce SD2			^{132}Ce SD3		
E_γ (keV)	I_γ	R	E_γ (keV)	I_γ	R	E_γ (keV)	I_γ	R
770.8(1)	10(1)	1.0(2)	724.4(1)	47(1)	0.9(2)	890.2(1)	50(2)	
809.3(1)	67(1)	0.9(2)	794.3(1)	70(2)	0.8(2)	949.6(1)	71(2)	1.2(4)
865.7(1)	76(1)	0.9(1)	865.9(1)	99(2)	0.8(2)	1017.5(1)	76(2)	
929.6(1)	$\equiv$100	1.0(1)	929.0(1)	97(2)	1.0(2)	1088.4(1)	72(2)	1.1(3)
995.9(1)	95(1)	1.0(1)	1000.8(1)	$\equiv$100	0.8(2)	1161.4(1)	84(2)	1.3(5)
1061.7(1)	89(1)	0.9(1)	1068.5(1)	80(2)	1.2(4)	1228.2(1)	90(2)	1.3(4)
1128.8(1)	82(1)	1.0(1)	1138.4(1)	86(2)	1.4(4)	1305.3(1)	$\equiv$100	1.0(3)
1196.4(1)	80(1)	1.0(2)	1211.3(1)	78(2)	0.8(2)	1383.5(1)	85(2)	0.9(3)
1265.6(1)	72(1)	1.0(2)	1288.5(1)	67(2)	1.1(2)	1465.4(1)	70(2)	0.9(3)
1336.8(1)	61(1)	1.0(2)	1364.5(1)	53(2)	1.6(4)	1541.1(2)	43(2)	0.7(3)
1410.7(1)	56(1)	0.9(2)	1453.9(2)	47(2)	1.6(4)	1611.5(2)	30(2)	0.8(3)
1488.1(1)	44(1)	1.0(2)	1538.3(2)	46(2)	1.6(4)	1665.4(3)	21(2)	
1569.4(2)	40(1)	1.0(2)	1621.5(2)	17(2)	1.1(3)	1735.6(3)	24(2)	
1654.9(2)	30(1)	1.0(2)	1730.1(3)	13(2)	1.4(3)	1815.2(3)	16(2)	
1743.9(2)	25(1)	1.1(2)	1816.1(3)	10(2)		1885.0(4)	17(2)	
1836.1(2)	21(1)	1.1(2)	1906.6(4)	9(2)		1953.7(4)	12(2)	
1931.0(2)	15(1)	1.1(2)	1998.9(5)	6(2)		2000.7(4)	12(2)	
2027.2(3)	9(1)	1.1(2)	2085.6(5)	5(2)		2054.2(5)	3(1)	
2122.8(4)	5(1)	1.6(5)						
2215.7(5)	3(1)							
2303(1)	2(1)							
2418(1)	$<$1							
2504(1)	$<$1							
2602(1)	$<$1							

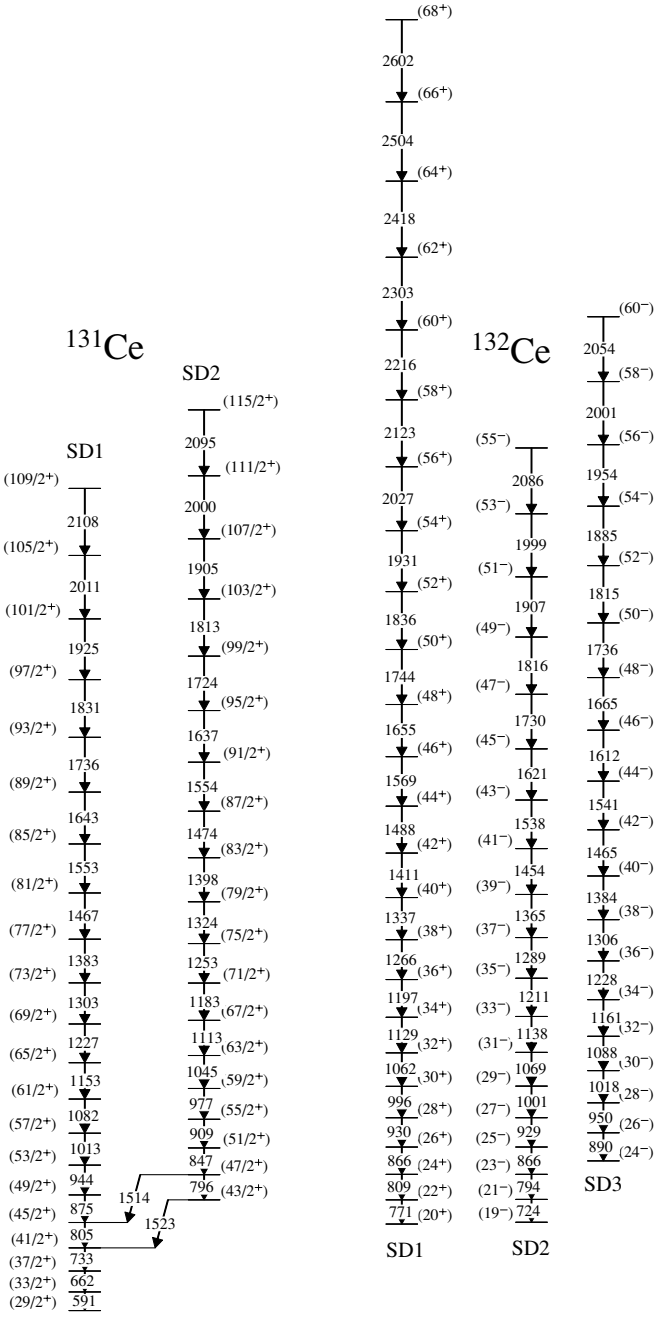

FIG. 5. The five SD bands in ^{131,132}Ce with assumed spin values.

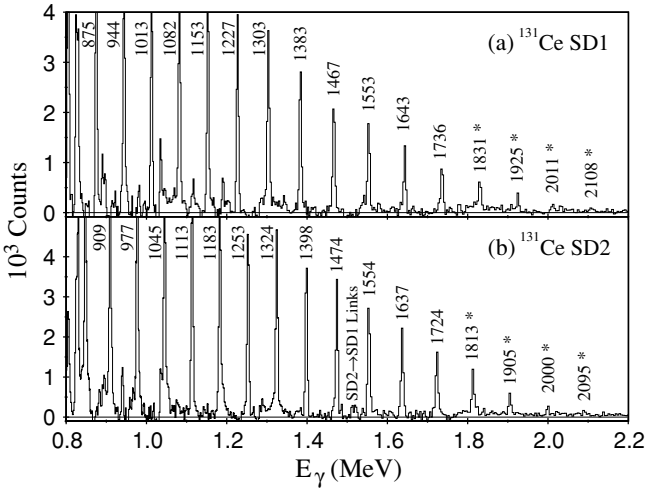

FIG. 6. Double-gated triple-coincidence spectra generated for the two SD bands in ^{131}Ce. Transition energies are labeled in keV, and the new transitions are marked with an asterisk.

III. DISCUSSION

Experimental dynamic moments of inertia $\Im = \partial I/\partial\omega$, which can be extracted without knowledge of the exact spin values, are plotted as a function of rotational frequency in Fig. 8 for the five SD bands in ^{131,132}Ce. In contrast to the other SD bands, SD2 and SD3 of ^{132}Ce tend to show more erratic behavior.

In order to interpret the behavior of the SD bands in ^{131,132}Ce at the highest spins, calculations have been performed in the framework of the configuration-constrained cranked Nilsson-Strutinsky (CNS) method without pairing [4,6,24], which has successfully described the smoothly terminating bands in the $A \sim 110$ region. Previous calculations on ^{131,132}Ce within the CNS formalism have been published in [7], and we refer the reader to this reference for a general description of the SD bands in this region. In the present paper, we concentrate on understanding the new experimental features, namely the

TABLE II. Measured γ-ray energies, relative intensities, and angular intensity ratios for the SD bands in ^{131}Ce. The absolute intensity of SD1 is ≈5% of the ^{132}Ce channel, while that of SD2 is ≈1%.

^{131}Ce SD1			^{131}Ce SD2		
E_γ (keV)	I_γ	R	E_γ (keV)	I_γ	R
591.5(1)	38(2)		795.5(1)	62(2)	0.8(2)
662.1(1)	79(2)	0.9(2)	847.4(1)	96(2)	0.8(2)
733.3(1)	84(2)	1.0(2)	908.6(1)	90(2)	1.0(2)
805.1(1)	≡100	0.9(2)	976.7(1)	≡100	1.0(2)
874.9(1)	92(2)	1.0(2)	1045.0(1)	89(2)	0.8(2)
944.0(1)	96(2)	0.9(2)	1113.1(1)	79(2)	1.2(2)
1012.5(1)	93(2)	0.8(2)	1182.9(1)	81(2)	1.3(2)
1081.8(1)	75(2)	1.0(2)	1252.9(1)	69(2)	1.1(2)
1152.9(1)	69(2)	0.9(2)	1324.4(1)	66(2)	1.1(2)
1226.7(1)	54(2)	1.1(2)	1398.1(1)	61(2)	1.1(2)
1303.4(1)	51(2)	1.1(2)	1474.0(1)	54(2)	1.0(2)
1383.3(1)	38(2)	1.1(2)	1553.9(1)	49(2)	1.1(2)
1466.6(1)	32(2)	1.1(2)	1636.6(2)	38(2)	1.2(2)
1553.4(1)	23(2)	1.2(2)	1723.5(2)	27(2)	1.1(2)
1643.2(2)	16(1)	1.2(2)	1813.4(3)	21(2)	1.1(2)
1735.8(2)	14(1)	1.0(2)	1905.3(3)	12(2)	1.3(3)
1830.5(3)	8(1)	1.0(2)	1999.6(4)	5(1)	0.8(3)
1925.0(3)	4(1)	1.0(3)	2094.6(5)	2(1)	
2011.0(3)	2(1)				
2108.4(4)	1(1)				
			SD2 → SD1 Links		
			1513.9(4)	6(1)	1.9(4)
			1522.6(4)	7(1)	1.9(3)

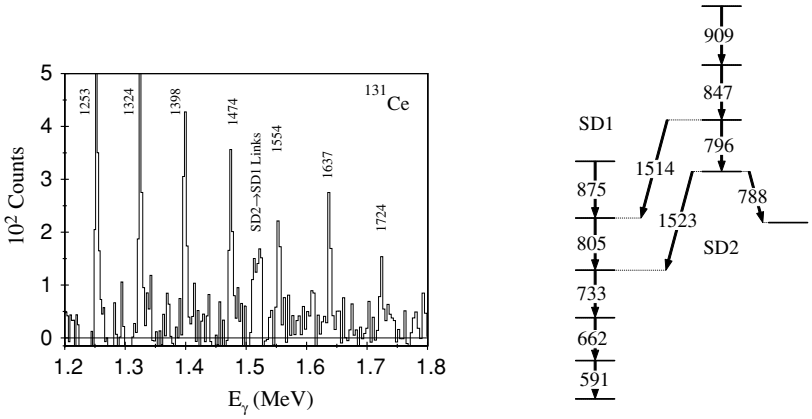

FIG. 7. Double-gated triple-coincidence spectrum (left) generated for ^{131}Ce showing the linking transitions, of energies 1514 and 1523 keV, between the two SD bands, and the depopulating 788-keV transition. A partial level scheme is shown to the right.

very high-spin part of SD1 in ^{132}Ce, and the relative spins and excitation energies of the two bands in ^{131}Ce.

It is convenient to label the configurations in ^{131,132}Ce relative to the $Z = 50$ and $N = 82$ closed cores, i.e., relative to the doubly magic ^{132}Sn nucleus. The configurations are thus labeled as $[p_1 p_2, n_1 n_2 n_3]$, where p_1 represents the number of $\pi g_{9/2}$ holes, p_2 the number of $\pi h_{11/2}$ particles, n_1 the number of $\nu h_{11/2}$ holes, n_2 the number of $\nu(h_{9/2}/f_{7/2})$ particles, and n_3 the number of $\nu i_{13/2}$ particles.

A. The superdeformed ^{132}Ce bands

As suggested in Ref. [7], the lower part of the experimental SD1 band in ^{132}Ce may be associated with the [24,422] configuration. More explicitly, this particular configuration can be expressed as $\pi[(g_{9/2})_8^{-2}(d_{5/2}/g_{7/2})_{12}^6(h_{11/2})_{16}^4]\ \nu[(h_{11/2})_{16}^{-4}(d_{5/2}/g_{7/2})_{10}^{-4}(d_{3/2}/s_{1/2})_2^{-4}(h_{9/2}/f_{7/2})_8^2(i_{13/2})_{12}^2]$, where we have specified the number of proton $(d_{5/2}/g_{7/2})$ particles and neutron $N_{\rm osc} = 4$ holes required to obtain the correct particle numbers, $Z = 58$ and $N = 74$. The $N_{\rm osc} = 4$ neutron holes are placed into the $s_{1/2}/d_{3/2}$ and $d_{5/2}/g_{7/2}$ subshells with no neutron holes in orbitals of $g_{9/2}$ character. The maximal spins of the pure configurations are given as subscripts; i.e., with the suggested distribution over subshells, this total configuration has a maximum spin of $I_{\rm max} = 8 + 12 + 16 + 16 + 10 + 2 + 8 + 12 = 84\hbar$. The corresponding calculated band is drawn in the upper panel of Fig. 9, where it is compared with the observed SD1 band, drawn in the lower panel. It can be seen that this band is calculated as yrast up to $I \approx 54\hbar$, but then it becomes strongly nonyrast for spin values beyond $I = 60\hbar$. Thus, it appears unlikely that the experimental SD1 band of ^{132}Ce, which is observed up to $I \approx 68\hbar$, can be assigned to this configuration in its *full spin range*. Indeed, in Ref. [7], it has already been suggested that in the higher spin region of the band, one neutron was excited from an orbital of $h_{11/2}$ character, to one of $h_{9/2}/f_{7/2}$ character, leading to a [24,532] configuration.

For a better understanding of the high-spin region of the observed SD1 band, the calculated [24,422], [24,532], and [24,642] even spin (signature $\alpha = 0$) bands, and one [24,532] odd spin ($\alpha = 1$) band, are shown in the upper panel of Fig. 9. These configurations with 10 $N_{\rm osc} = 5$ neutrons have their $I_{\rm max}$ values in the range 84–92$\hbar$. If the observed band should be assigned to one of these pure configurations, the two low-lying [24,532] bands [labeled $(h_{9/2}/f_{7/2})^3_-$] having even or odd spins appear to be the only possible candidates. However, there is also the possibility that the configuration is

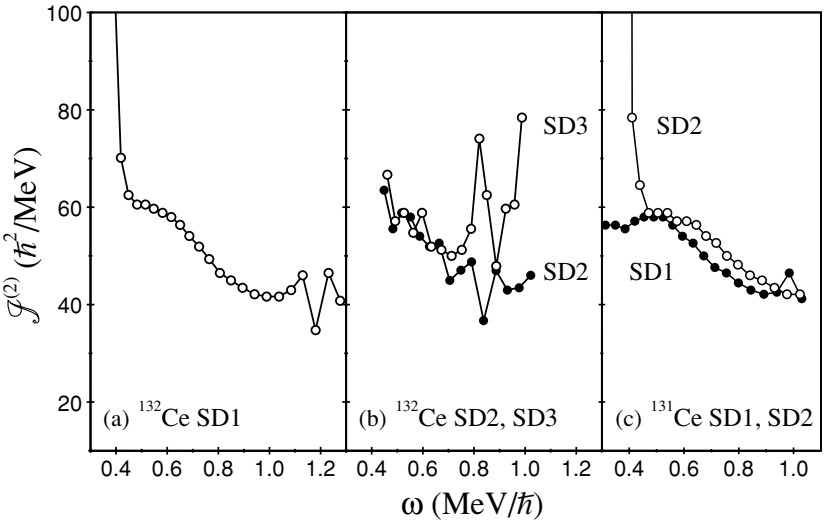

FIG. 8. Experimental dynamic moments of inertia $\Im^{(2)}$ for the five SD bands in ^{131,132}Ce plotted as a function of rotational frequency ω.

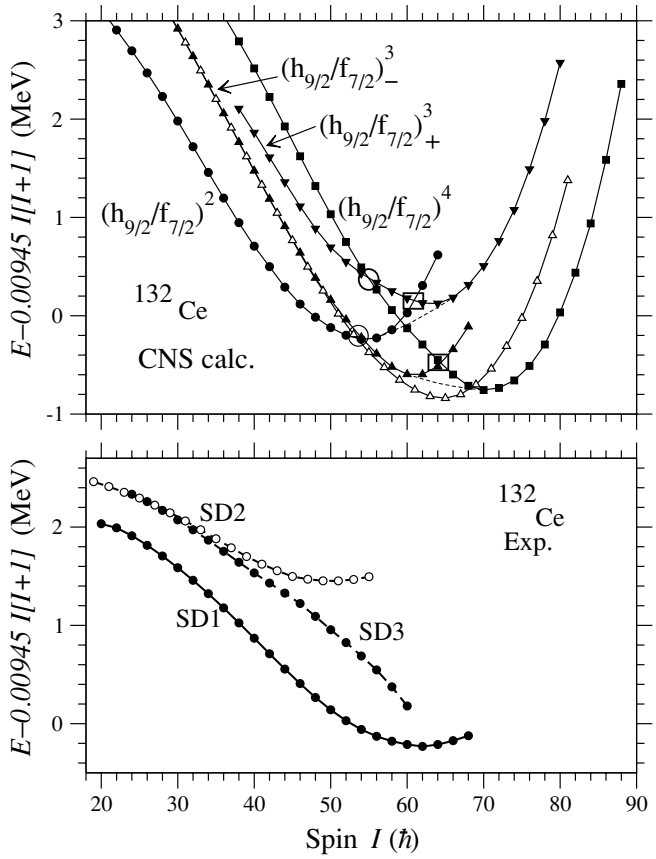

FIG. 9. The excitation energy relative to a rigid rotor reference as a function of spin for ^{132}Ce. The superdeformed bands in ^{132}Ce are drawn in the lower panel and compared with calculated bands of the type $\pi(g_{9/2})^{-2}(h_{11/2})^4\nu(i_{13/2})^2$ in the upper panel. The calculated bands have different distributions of the 10 $N_{\rm osc} = 5$ neutrons over the orbitals of $h_{11/2}$ and $h_{9/2}/f_{7/2}$ character, where the number of the latter is indicated for the different bands together with their signature if the number is odd. Specific crossings caused by crossings between single-particle orbitals, as illustrated in Fig. 10, are indicated by circles and rectangles. In the case of strong interaction, suggested mixing between "pure" configurations is indicated by dashed lines. The observed SD1 band is drawn with the assumption that the state which is fed by the 771-keV transition has $I^\pi = 20^+$, but its excitation energy is not known, i.e., only the shapes, but not the absolute values, of the experimental and calculated curves should be compared. The suggested signature degeneracy at low spins for the SD2 and SD3 bands is only tentative.

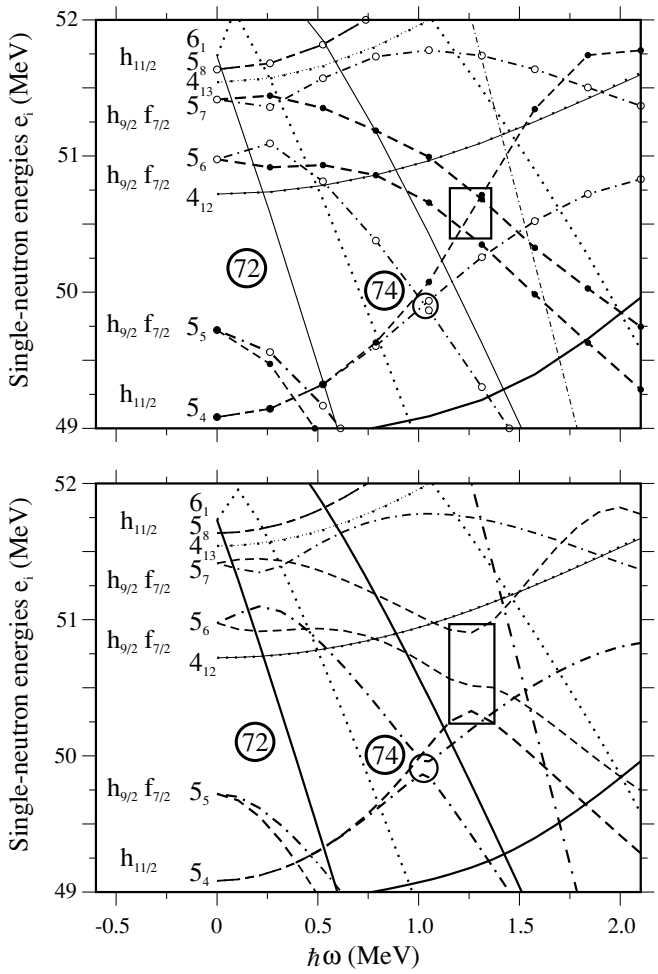

FIG. 10. Neutron single-particle orbitals as functions of rotational frequency ω at a typical deformation around $I = 60\hbar$ for the [24,422] and [24,532] configurations in ^{132}Ce ($\varepsilon_2 = 0.344$, $\varepsilon_4 = 0.040$, $\gamma = 5.5^\circ$). The orbitals are labeled by their $N_{\rm osc}$ shells, and the ordering within the $N_{\rm osc}$ shell is shown a subscript. For the $N_{\rm osc} = 5$ orbitals, the j shells which dominate their wave functions at $\omega = 0$ are also indicated. The $N_{\rm osc} = 5$ orbitals are shown by thick dashed lines with solid ($\alpha = 1/2$) circles or dot-dashed lines with open ($\alpha = -1/2$) circles, while the even parity orbitals are shown by thin, solid ($\alpha = 1/2$) lines or dotted ($\alpha = -1/2$) lines. In the lower panel, the orbitals are drawn as they come out from the diagonalization, while in the upper panel, real crossings have been formed between orbitals which interact and exchange character in a limited spin interval. Crossings that are important for the bands in Fig. 9 are indicated by a circle and a rectangle, respectively.

different at low- and high-spin values, as mentioned above. To investigate this in more detail, single-neutron routhians are drawn in Fig. 10 at a deformation relevant for $I \approx 60\hbar$ for these ^{132}Ce configurations. In the upper panel, the interaction between the $h_{11/2}$ and $h_{9/2}/f_{7/2}$ orbitals has been removed, i.e., crossings have been formed resulting in orbitals which develop smoothly as a function of rotational frequency. However, to illustrate the interaction strength at the different crossings, the orbitals are drawn in the lower panel as they come out from the diagonalization. There will always be some interaction between all $N_{\rm osc} = 5$ orbitals, so two $N_{\rm osc} = 5$ orbitals having the same signature are not allowed to cross. The orbital labeled 5_4 is of $h_{11/2}$ character, and it crosses orbitals of $h_{9/2}/f_{7/2}$ character at three different frequencies (see upper panel). At the first crossing at $\omega \approx 0.4$ MeV/$\hbar$, the interaction strength has almost vanished, as seen in the lower panel, so creating a crossing is clearly justified in this case. At the second crossing between the $\alpha = -1/2$ orbitals at $\omega \approx 1.0$ MeV/$\hbar$, the interaction strength is much stronger but can still be approximated to a real crossing. Finally, there is a "crossing" with two $\alpha = 1/2$ orbitals at $\omega = 1.2$–1.3 MeV/$\hbar$. In this case, the interaction strength is quite strong, so it

is probably most realistic not to create a crossing, i.e., the orbital will slowly change character from $h_{11/2}$ to $h_{9/2}/f_{7/2}$. It would then correspond to a gradual transition between two bands in Fig. 9, as shown by the dashed line. The two single-particle crossings at $\omega = 1.0$–1.3 MeV/$\hbar$ in Fig. 10, and the corresponding band crossings in Fig. 9, are encircled and framed, respectively.

Compared with experiment, the agreement with the band which starts as $(h_{9/2}/f_{7/2})^2$ and then follows the dashed line, gradually becoming $(h_{9/2}/f_{7/2})^3$ around $I = 60\hbar$, appears quite good (note that this interpretation is somewhat different from that of Ref. [7], where it was suggested that the transition to an $(h_{9/2}/f_{7/2})^3$ configuration has already occurred at the encircled crossing around $I \approx 54\hbar$). In the present approach, we are not able to describe the details of the band crossings, but we can note that the $\Im^{(2)}$ moment of inertia of the observed band, shown in Fig. 8(a), shows an irregularity around $\omega \sim 1.2$ MeV/$\hbar$ ($I \sim 60\hbar$), which would be expected from the calculated crossings between different bands with 10 $N_{\rm osc} = 5$ neutrons shown in Fig. 9.

An alternative interpretation is that the observed SD1 band has a $(h_{9/2}/f_{7/2})^3$ configuration at low spin, and following the dashed line in Fig. 9, gradually evolves into the $(h_{9/2}/f_{7/2})^4$ configuration in the $I = 60$–$70\hbar$ spin range. This interpretation has the advantage that the band is calculated as yrast or close to yrast for spin values $I = 60$–$70\hbar$, which would be expected considering that it is seen experimentally in this region. However, features making this interpretation less likely are that these bands are calculated rather high above yrast for low-spin values, and that two signature-degenerate bands are predicted over an extended spin range up to $I \approx 55\hbar$; in contrast, no signature partner to the SD1 band has been experimentally observed.

The calculated bands drawn in Fig. 9 have $I_{\rm max}$ values in the range $I = 84$–$92\hbar$, i.e., if their configurations could really be described as protons or neutrons in the j shells (or groups of j shells) listed above, they would terminate in axially symmetric states at their respective $I_{\rm max}$ values. Indeed, there will be a competition between the tendencies leading to smaller deformations, with more pure j shells and termination, and the tendencies to mix the j shells so that the deformations remain large and the bands never terminate. These latter effects will dominate for the configurations shown in Fig. 9, so possible terminations will occur far beyond the $I_{\rm max}$ values. However, when the spin value approaches $I_{\rm max}$, the energy curves show similar features [4], as is observed for smoothly terminating bands, i.e., they show strong upslopes when drawn relative to a rigid rotation reference. The feature that the $\Im^{(2)}$ value decreases when bands approach their $I_{\rm max}$ values was also deduced from more general considerations in Ref. [2], although it should be noted that $I_{\rm max}$ was calculated in a somewhat different way, and the distribution of particles over different j shells within one $N_{\rm osc}$ shell was not considered.

The other two superdeformed bands in ^{132}Ce, SD2 and SD3, are also drawn in the lower panel of Fig. 9, while their $\Im^{(2)}$ moments of inertia are shown in Fig. 8(b). Since their exact spin values are not known, it is difficult to give definitive configuration assignments. The SD2 band shows properties

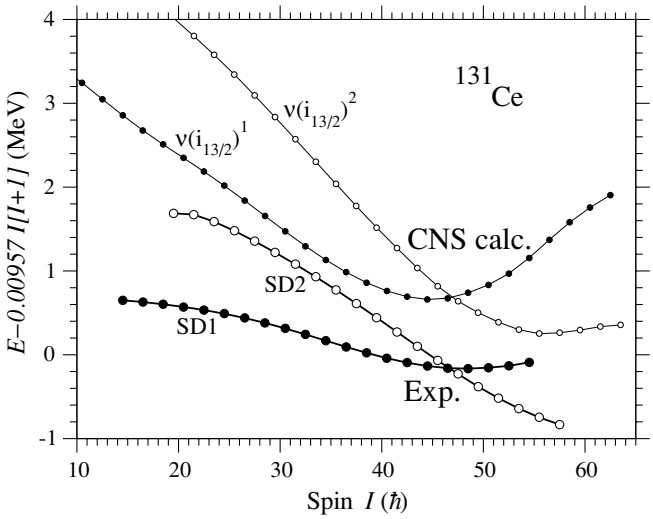

FIG. 11. The excitation energy relative to a rigid rotor reference as a function of spin for the two bands observed in ^{131}Ce compared with the calculated bands having the [24,421] and [24,422] configurations, i.e., the two bands differ by a $(N_{\rm osc} = 4)^{-1}(i_{13/2})^1$ neutron excitation. The relative energies between experiment and calculations are not known, but the relative energy between the two observed and calculated bands, respectively, supports the present assignment.

somewhat similar to those of the SD1 band, e.g., the $\Im^{(2)}$ moment of inertia decreases on average with increasing spin. Therefore, it might also be built from the bands shown in the upper panel. The SD3 band, on the other hand, is much more downsloping in Fig. 9, corresponding to a $\Im^{(2)}$ which rather increases on average at the highest spin values. The irregular behavior of $\Im^{(2)}$ (Fig. 8) suggests one or two band crossings, which again might be formed from the bands drawn in the upper panel, or maybe some similar configuration with negative parity, which might be formed with one $N_{\rm osc} = 5$ neutron excited to the 4_{12} orbital (see Fig. 10). Another possibility is that this band has one proton excited to $N_{\rm osc} = 6$ (or possibly a third neutron excited to $N_{\rm osc} = 6$) at the highest spin values. Such configurations are calculated to come into the yrast region around $I = 60\hbar$. It would explain the strong downslope in Fig. 9, but one would then expect a sharp band crossing when the $N_{\rm osc} = 6$ orbital becomes occupied, which is not seen in the SD3 band.

B. The superdeformed ^{131}Ce bands

The second (SD2) band in ^{131}Ce is "identical" to the SD1 band in ^{132}Ce, i.e., their $\Im^{(2)}$ moments of inertia, shown in Fig. 8, are similar, and the effective alignment [25,26] between these two bands is very close to zero (see Fig. 8 of Ref. [7]). This suggests that the band in ^{131}Ce has a hole in an orbital with a small and almost constant $\langle j_x \rangle$. As already concluded in Ref. [7], the only reasonable candidate is the $N_{\rm osc} = 4$, [411] 1/2 orbital, which is dominated by the $d_{3/2}$ subshell. It corresponds to the solid line, which comes up into Fig. 10 at $\omega \approx 0.75$ MeV/$\hbar$. At small frequencies, its $\langle j_x \rangle$ value is

small, which is consistent with small effective alignment. The SD2 band in ^{131}Ce is linked to the SD1 band, so the relative spins of the two bands are known. It turns out that SD2 has a considerably larger alignment than SD1, but the same parity. This strongly suggests that SD1 is formed from SD2 by removing the second $N_{\rm osc} = 6$ neutron and placing it in the [411]1/2 orbital. The two bands in ^{131}Ce would then be assigned as [24,421] and [24,422], respectively. They are calculated to be yrast in their respective spin groups for $I = 24$–$46\hbar$ (SD1) and $I = 35$–$51\hbar$ (SD2), and they are compared with the observed bands in Fig. 11. The observed bands are assigned spin values consistent with those used for SD1 in ^{132}Ce in Fig. 9. In general, the agreement between experimental and calculated values is very good. Because the observed spins in ^{131}Ce are lower than those in ^{132}Ce, we need not consider how the $h_{11/2}$ and $(h_{9/2}/f_{7/2})$ orbitals cross at high frequencies in this case. One could note, however, that if the low-spin part of the SD1 band in ^{132}Ce has the alternative [24,532] configuration, this would also work for the ^{131}Ce bands, i.e., the relative properties of the bands in ^{131}Ce would be essentially the same if their $N_{\rm osc} = 5$ neutrons were distributed as $(h_{11/2})^{-5}(h_{9/2}/f_{7/2})^3$ instead of as $(h_{11/2})^{-4}(h_{9/2}/f_{7/2})^2$.

IV. CONCLUSIONS

By using the EUROBALLγ-ray spectrometer in conjunction with the inner-ball calorimenter, is has been possible to extend the superdeformed bands in ^{131,132}Ce to higher spin. In particular, the yrast SD band of ^{132}Ce now spans an impressive $50\hbar$ and shows properties of smooth band termination at the highest spin, $\sim 70\hbar$, which represents one of the highest spins ever observed in the atomic nucleus. Configurations have been suggested for the SD bands through comparison with cranked Nilsson-Strutinsky calculations. The proposed structures of the SD bands in ^{131,132}Ce, involving holes in the $\pi g_{9/2}$ orbital, establish a link between the prevalent $A \sim 110$ terminating bands and the superdeformed bands in the $A \sim 130$ mass region; the presence of holes in the $\pi g_{9/2}$ extruder orbital is of great importance in creating enhanced deformation in the two mass regions. However, even though the ^{131,132}Ce have several properties in common with the terminating bands in the $A \sim 110$ region, they are far away from any real termination into a noncollective oblate state.

Despite the present high-statistics, high-fold data sets, it has not been possible to definitely link any of the five SD bands in ^{131,132}Ce into their low-spin, lesser deformed structures. This may suggest that the decay of these SD bands is fragmentary, caused by a substantial potential energy barrier between the two shapes in the cerium isotopes. Clear links have, however, been established between the two SD bands in ^{131}Ce, thus fixing their relative excitation energies and spins.

ACKNOWLEDGMENTS

The EUROBALL project is a joint European venture funded by several countries. This work was also funded by European Commission contracts TMR:ERBFMGECT980145 and EUROVIV:HPRI-CT-1999-00078, the UK Engineering and Physical Sciences Research Council, the Hungarian Scientific Research Fund OTKA (contract number T046901), and the Swedish Science Research Council.

[1] T. Troudet and R. Arvieu, Phys. Lett. **B82**, 308 (1979); Z. Phys. A **291**, 183 (1979).
[2] I. Ragnarsson, Phys. Lett. **B199**, 317 (1987).
[3] I. Ragnarsson, Z. Xing, T. Bengtsson, and M. A. Riley, Phys. Scripta **34**, 651 (1986).
[4] A. V. Afanasjev, D. B. Fossan, G. J. Lane, and I. Ragnarsson, Phys. Rep. **322**, 1 (1999).
[5] I. Ragnarsson, V. P. Janzen, D. B. Fossan, N. C. Schmeing, and R. Wadsworth, Phys. Rev. Lett. **74**, 3935 (1995).
[6] A. V. Afanasjev and I. Ragnarsson, Nucl. Phys. **A591**, 387 (1995).
[7] A. V. Afanasjev and I. Ragnarsson, Nucl. Phys. **A608**, 176 (1996).
[8] P. J. Nolan, A. J. Kirwan, D. J. G. Love, A. H. Nelson, D. J. Unwin, and P. J. Twin, J. Phys. G **11**, L17 (1985).
[9] A. J. Kirwan, G. C. Ball, P. J. Bishop, M. J. Godfrey, P. J. Nolan, D. J. Thornley, D. J. G. Love, and A. H. Nelson, Phys. Rev. Lett. **58**, 467 (1987).
[10] D. Santos, J. Gizon, C. Foin, J. Genevey, A. Gizon, M. Józsa, J. A. Pinston, C. W. Beausang, S. A. Forbes, P. J. Nolan, E. S. Paul, A.T. Semple, J. N. Wilson, R. M. Clark, K. Hauschild, R. Wadsworth, J. Simpson, B. M. Nyakó, L. Zolnai, W. Klamra, N. El Aouad, and J. Dudek, Phys. Rev. Lett. **74**, 1708 (1995).
[11] Y.-X. Luo, J.-Q. Zhong, D. J. G. Love, A. Kirwan, P. J. Bishop, M. J. Godfrey, I. Jenkins, P. J. Nolan, S. M. Mullins, and R. Wadsworth, Z. Phys. A **329**, 125 (1988).
[12] Y. He, M. J. Godfrey, I. Jenkins, A. J. Kirwan, P. J. Nolan, S. M. Mullins, R. Wadsworth, and D. J. G. Love, J. Phys. G **16**, 657 (1990).
[13] A. T. Semple, P. J. Nolan, C. W. Beausang, S. A. Forbes, E. S. Paul, J. N. Wilson, R. Wadsworth, K. Hauschild, R. M. Clark, C. Foin, J. Genevey, J. Gizon, A. Gizon, J. A. Pinston, D. Santos, B. M. Nyako, L. Zolnai, W. Klamra, and J. Simpson, Phys. Rev. C **54**, 425 (1996).
[14] F. A. Beck, Prog. Part. Nucl. Phys. **28**, 443 (1992).
[15] J. Simpson, Z. Phys. A **358**, 139 (1997).
[16] I. Y. Lee, Nucl. Phys. **A520**, 641c (1990).
[17] D. C. Radford, Nucl. Instrum. Methods A **361**, 297 (1995).
[18] D. C. Radford, M. Cromaz, and C. J. Beyer, in *Proceedings of the Nuclear Structure '98 Conference, Gatlinburg, 1998*, edited by C. Baktash (American Institute of Physics, New York, 1999, CP481), p. 570.
[19] K. Lagergren (private communication).
[20] B. Crowell, M. P. Carpenter, R. G. Henry, R. V. F. Janssens, T. L. Khoo, T. Lauritsen, and D. Nisius, Nucl. Instrum. Methods A **355**, 575 (1995).
[21] P. T. W. Choy, Ph.D. thesis, University of Liverpool, 2003.
[22] E. S. Paul, A. J. Boston, D. T. Joss, P. J. Nolan, J. A. Sampson, A. T. Semple, F. Farget, A. Gizon, J. Gizon, D. Santos, B. M.

Nyakó, N. J. O'Brien, C. M. Parry, and R. Wadsworth, Nucl. Phys. **A619**, 177 (1997).
[23] W. Nazarewicz, P. J. Twin, P. Fallon, and J. D. Garrett, Phys. Rev. Lett. **64**, 1654 (1990).
[24] T. Bengtsson and I. Ragnarsson, Nucl. Phys. **A436**, 14 (1985).
[25] F. S. Stephens, M. A. Deleplanque, J. E. Draper, R. M. Diamond, A. O. Macchiavelli, C. W. Beausang, W. Korten, W. H. Kelly, F. Azaiez, J. A. Becker, E. A. Henry, S. W. Yates, M. J. Brinkman, A Kuhnert, and J. A. Cizewski, Phys. Rev. Lett. **65**, 301 (1990).
[26] I. Ragnarsson, Nucl. Phys. **A557**, 167 (1993).